AIAA 81-1661R

Flow Visualization Reveals Causes of Shuttle Nonlinear Aerodynamics

J. Peter Reding* and Lars E. Ericsson†
Lockheed Missiles and Space Company, Inc., Sunnyvale, California

Selected oil-flow photographs, which show many of the complicated flow phenomena that have dominated the aerodynamic characteristics of the various Space Shuttle configurations, are presented and analyzed. The analysis covers the entire spectrum of Shuttle configurations from the early straight wing, fully recoverable orbiter and booster to the current double delta planform orbiter. For all the cases analyzed, the oil-flow photographs reveal that flow separation is the fundamental cause of the nonlinear aerodynamic characteristics. The success of these simple techniques in revealing the causes at the Shuttle nonlinear aerodynamics underscores their usefulness for other aircraft configurations dominated by flow separation and/or flow interference effects.

Nomenclature

a = speed of sound
c = reference length, mean aerodynamic chord
c.p. = center of pressure
l = rolling moment; coefficient, $C_l = l/\bar{q}S$
M = Mach number $= U/a$
m = pitching moment; coefficient, $C_m = m/\bar{q}Sc$
N = normal force; coefficient, $C_N = N/\bar{q}Sc$
n = yawing moment; coefficient, $C_n = n/\bar{q}Sc$
p = local pressure; coefficient, $C_p = (p - p_\infty)/\bar{q}$
q = pitch rate
$\bar{q}$ = freestream dynamic pressure $= \rho U^2/2$
S = reference area, exposed wing area
t = time
U = freestream velocity
α = angle of attack
$\dot{\alpha}$ = pitch rate $= \partial\alpha/\partial t$
β = sideslip angle
δ = control deflection
ρ = freestream air density

Subscripts

q = $\partial/\partial(qc/U)$
U = upper wing pressures
α = $\partial/\partial\alpha$
$\dot{\alpha}$ = $\partial/\partial(\dot{\alpha}c/U)$
β = $\partial/\partial\beta$
∞ = freestream conditions

Introduction

ALTHOUGH the Shuttle is a lifting vehicle, it always has been intended that it re-enter as a ballistic re-entry body. That is, the orbiter re-enters at a very high angle of attack, producing very large drag for rapid deceleration in the upper, tenuous portion of the atmosphere. This drag reduces the velocity of the orbiter in the dense, low altitude region of the atmosphere, and avoids the very high heat transfer rates produced by high velocities in dense air.

Because of the high re-entry angle of attack, only the orbiter bottom is exposed to the direct impingement of the freestream flow, thus restricting the need for significant heat protection to the orbiter bottom. The leeside, being submerged in the relatively cool separated flow wake, needs comparatively little heat protection; thus heatshield weight is minimized.

However, oil-flow data presented herein reveal that the leeside of the orbiter is never completely stalled. This, together with control induced separation effects, are shown to be responsible for the Shuttle's nonlinear aerodynamics.

Straight Wing Orbiter

The straight wing orbiter and booster were both designed to re-enter at 60-deg angle of attack in order to maintain totally separated flow on the orbiter leeside. Oil-flow photographs showed that regions of flow reattachment occur on the fuselage sides and on the vertical tail (Fig. 1a).[1,2] These flow reattachment regions can be seen to emanate from the wing-fuselage and horizontal tail-fuselage junctures, evidently caused by the vortices generated at the wing- and tail-fuselage junctures. These vortices can be described as "vortical jets" resulting from the merged wing- and tail-fuselage corner flows. These vortices entrain the freestream flow and direct it to the fuselage sides and to the vertical tail, causing the imbedded regions of flow reattachment evident in the otherwise separated flow (Fig. 1). As the vehicle is yawed, the vortex induced reattachment regions become unsymmetric, causing a nonlinear, wing induced tail load at hypersonic speeds (Fig. 1). At lower speeds, the reattachment occurs suddenly, causing discontinuous yaw stability with attendant hysteresis effects (Fig. 1). The source is revealed in the oil-flow photographs, which also suggest a fix for the problem. It is obvious that large fillets in the wing-fuselage juncture would mitigate or eliminate the discontinuous yaw characteristics. Without the oil-flow data, the causes of the nonlinear yaw stability would be a mystery, and insight would be lacking to suggest a fix for the problem of discontinuous yaw characteristics.

Delta Planform Orbiters

The delta body orbiter also experiences vortex-tail interference effects.[2] The delta body leading edge vortices, by following the leading edges of the rolled-out tail surfaces, generated coupled pitch-yaw nonlinearities. One can see the beginning of leading edge vortex formation over the rolled out fins at $\alpha = 10$ deg (Fig. 2a). The stability characteristics show the development of a nonlinear increase in pitch stability as the leading edge vortices develop on the fins, increasing leeside suction pressures for 8 deg $\leq \alpha \leq 16$ deg (Fig. 2b). The unstable nonlinearity at $\alpha > 16$ deg results from the loss in suction pressures under the burst vortex. When the body is yawed at angles of attack between 8 and 16 deg, the strength of the vortex increases on the upwind tail surface; this causes greater suction pressures on the inside of that fin; correspondingly less suction is generated on the inside of the

Presented as Paper 81-1661 at the AIAA Aircraft Systems and Technology Conference, Dayton, Ohio, Aug. 11-13, 1981; submitted Aug. 20, 1981; revision received Jan. 28, 1982. Copyright © American Institute of Aeronautics and Astronautics, Inc., 1981. All rights reserved.

*Staff Engineer. Associate Fellow AIAA.
†Senior Consulting Engineer. Associate Fellow AIAA.

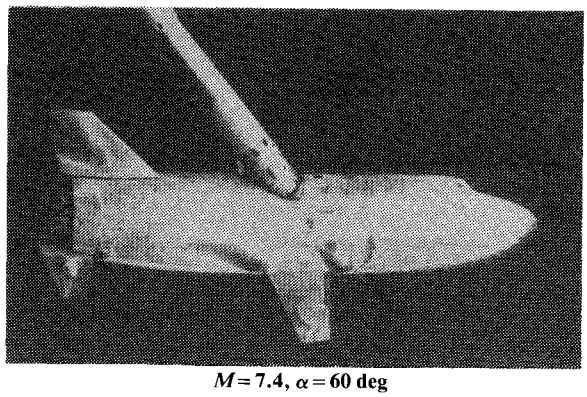

$M = 7.4$, $\alpha = 60$ deg

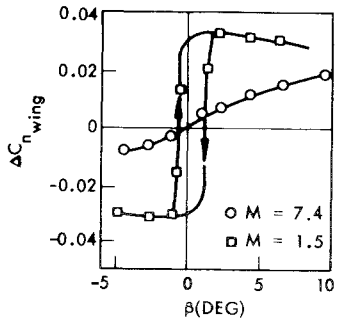

Fig. 1 Vortex interference effects on an early straight wing orbiter.

opposite (downwind) fin. Thus there is a tendency for the leading edge vortices over the fins to give a stabilizing increment in the yaw stability with increasing angle of attack (Fig. 2c).

Delta Wing Orbiter

For the delta wing (phase B) orbiters, the re-entry angle of attack was decreased to approximately 30 deg for most of the hypersonic speed range, where it remains today. Significant regions of attached flow occur on the leeside of the delta wings in this angle-of-attack range, as indicated by oil being scrubbed off the wings near the leading edge (Fig. 3).[3] Cross[4] classified the various types of leeside flow on delta wings, three of which are applicable to the Shuttle. At low angles of attack, the flow component normal to the leading edge must be turned parallel to the freestream near the center of the wing (for a pure delta wing); this is accomplished by means of a Mach wave. When the angle of attack is great enough to cause a detached leading edge (bow) shock, the embedded leeside shock becomes strong enough to separate the boundary layer; that is, the subsonic flow over the leading edge expands to reach supersonic speeds on the leeside of the wing. Thus the downstream turning is accomplished by a strong shock (a normal shock in the plane of the flow normal to the leading edge), which causes flow separation. As the angle of attack is further increased, the leeside boundary layer is weakened, the pressure gradient becomes more adverse, and the shock strength becomes greater, all because of increased leeside expansion. These effects combine to promote the growth of the separated flow region with increasing angle of attack, until eventually the entire leeside of the wing is stalled.

The phenomenon of wing leading edge shock detachment causes a complete readjustment of the wing loads.[5] Shock detachment results in a subsonic leading edge and a sudden realization of leading edge suction pressures (inset sketches in Fig. 4a). The leading edge suction increases wing lift, which gives a more stable pitching moment. In addition, there is a lift reduction inboard of the shock in the separated flow region. Because of the ogee wing planform, these two effects combine to generate a statically stabilizing force couple, since the center of pressure of the lift loss is forward of the center of pressure of the suction effect. The result of the suction effect

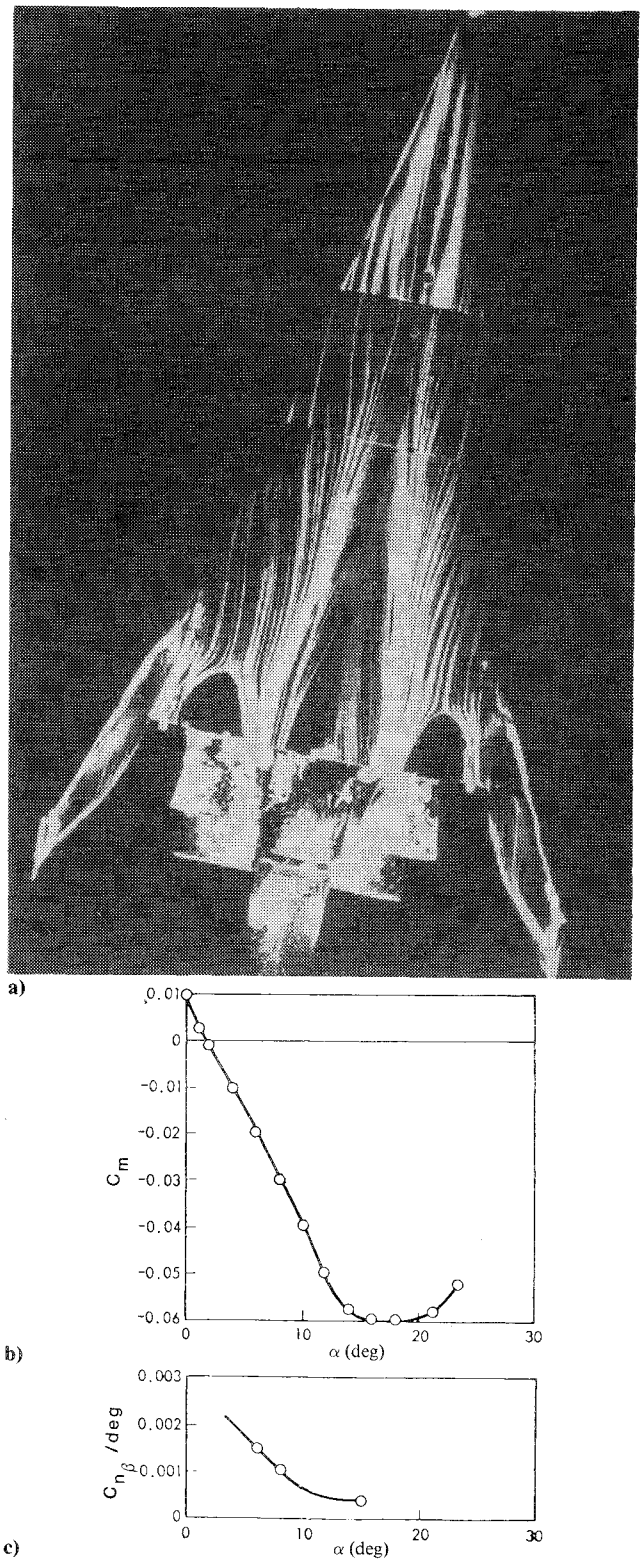

Fig. 2 Vortex interference on the delta body orbiter. a) $\alpha = 10$ deg, $M = 1.0$. b) Pitch stability ($M = 1.0$). c) Yaw stability ($M = 1.0$).

is a nonlinearity in the pitching moment that correlates with the angle of attack of shock detachment (Fig. 4).

Control Induced Effects

Oil-flow studies were used to investigate the effects of control deflection on the stability of an early NASA designed, 60-deg delta wing (040A) orbiter.[6] Only the left elevon was deflected to emphasize the effects of controls on both the stability characteristics and the oil-flow patterns. Control effects can be seen by comparing the left wing oil-flow pat-

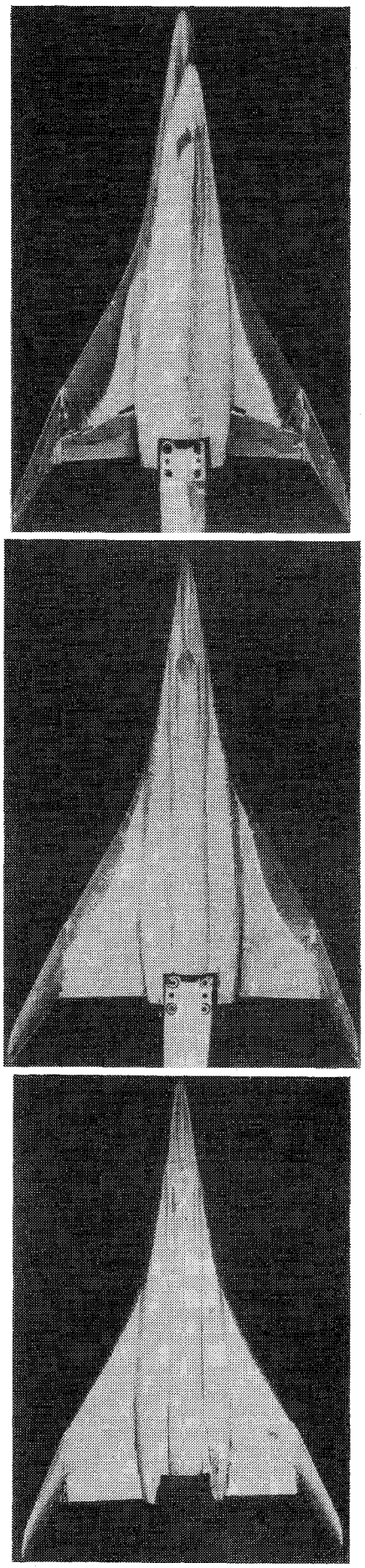

a)

b)

c)

Fig. 3 Hypersonic leeside flow patterns, delta wing orbiter, $M=7.4$. a) $\alpha=15$ deg, $\beta=-5$ deg. b) $\alpha=30$ deg, $\beta=0$ deg. c) $\alpha=45$ deg, $\beta=0$ deg.

terns with those on the right wing which are uncomplicated by control deflection effects.

Generally, strong coupling was observed between pitch, yaw, and roll degrees of freedom, caused primarily by interference with the "box car" fuselage (Fig. 5). The wing flow dominates not only the nonlinear pitch characteristics, but the nonlinear lateral-directional characteristics as well; this is revealed by the oil-flow photographs (Fig. 6). At low angles of attack ($\alpha=6$ deg), the wing flow is attached, as the nearly streamwise oil streaks indicate (Fig. 6a). Between $\alpha=6$-10 deg, a leading edge vortex begins to form, indicated by the converging oil streaks along the wing leading edge (Fig. 6b). Although the normal force is unaffected by the leading edge vortex formation, a small stable nonlinearity in C_m develops

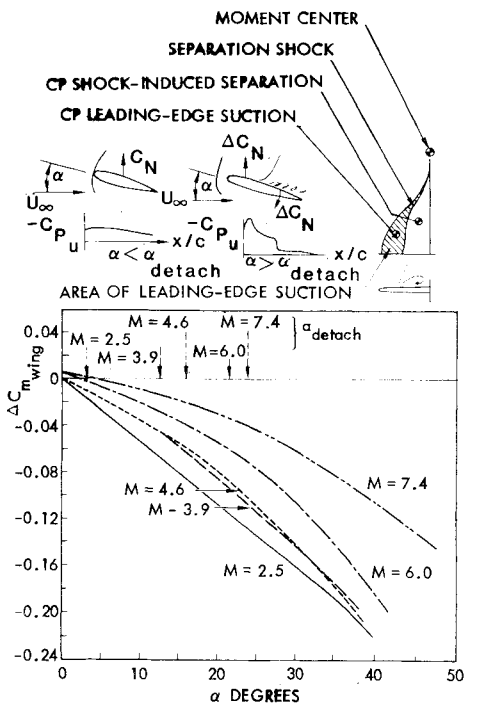

Fig. 4 Effect of leading edge shock detachment on the stability of a delta wing orbiter.

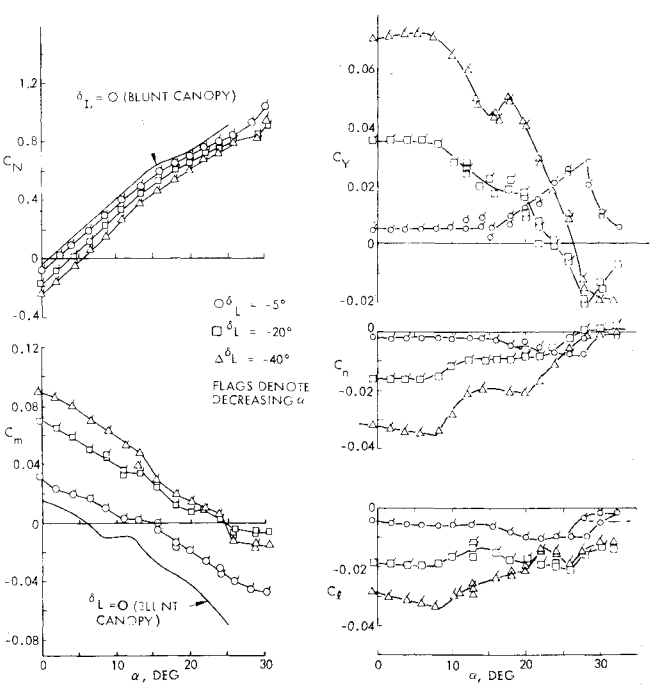

Fig. 5 Stability of the NASA designed (040A) orbiter at $M=0.9$.

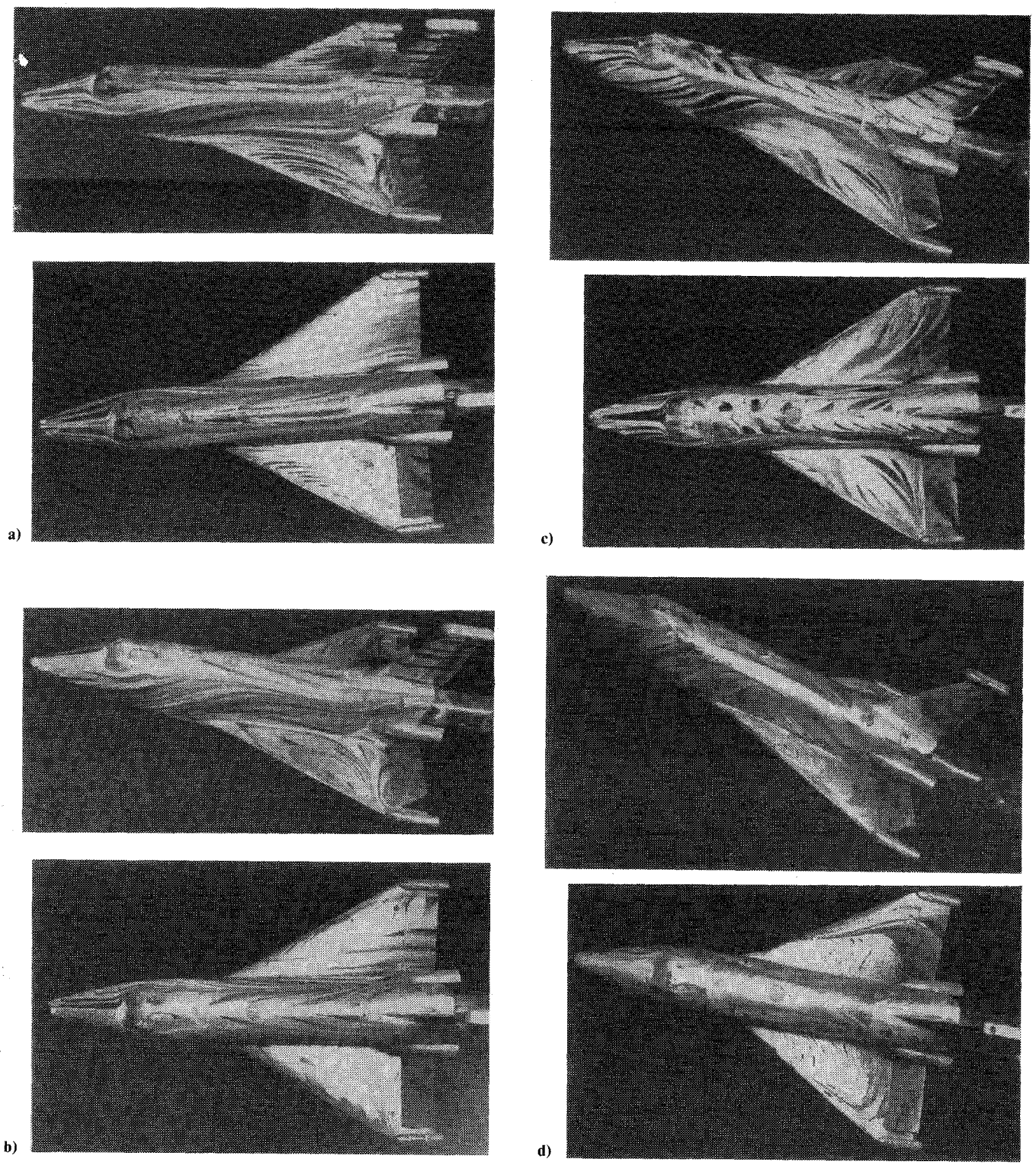

Fig. 6 Oil-flow patterns on the NASA designed (040A) orbiter. a) $\alpha = 6$ deg. b) $\alpha = 10$ deg. c) $\alpha = 20$ deg. d) $\alpha = 30$ deg.

for $\alpha > 6$ deg (particularly for $\delta_L = 0$ and -5 deg, Fig. 5). The plateau in C_m for 10 deg $\leq \alpha \leq 15$ deg is the result of leeside vortex formation over the topside of the fuselage, as indicated by the feather-like divergent reattachment lines along the topside of the fuselage (Figs. 6b-d). The effect is destabilizing because the vortex induced suction is centered forward of the moment reference point. This leeside vortex effect is not associated with the closed separation bubble on the cabin top, at all α. This bubble is vented via a pair of counterrotating vortices on the cabin top that are evident in all of the oil-flow photographs.

Vortex burst begins to develop for $\alpha \geq 15$ deg, explaining the gradual reduction of the stable C_m slope and the nonlinearity in the C_N curves that begins at $\alpha = 15$ deg. Vortex burst is indicated by the loss in the well-defined separation line over the outer third of the wing leading edges accompanied by a strong spanwise flow over the tip (Fig. 6c). Eventually, as α is further increased, the entire wing flow is dominated by vortex burst, as indicated by the reverse flow on the wings (Fig. 6d).

When the wing flow is attached, the control effects on the lateral-directional stability characteristics are fairly insensitive to angle of attack (Fig. 5). As the leading edge vortex develops (between $\alpha = 6$ and 10 deg), the control-induced separation begins to shrink for $\delta_L = -40$ deg (compare Figs. 6c and 6b), and for $\delta_L = -20$ deg as well, causing C_Y, C_n, and

C_l to approach zero (Fig. 5). The elevon induced flow separation occurs on both the wing and fuselage, coupling C_l, C_Y, and C_n with one another. Sidewash induced over the aft fuselage and tail (e.g., Figs. 6a and 6b) contributes to this coupling. The leading edge vortex reduces the flow separation by bleeding off the weakened boundary layer flow over the wing, particularly from the wing-fuselage juncture. The resulting stronger boundary layer is more difficult to separate, and the elevon induced separation shrinks. The similarity between the $\delta_L = -20$ deg and the $\delta_L = -40$ deg lateral-directional characteristics is indicative of similar flow phenomena. However, no flow separation occurs for $\delta_L = -5$ deg, and the lateral-directional characteristics are unaffected by leading edge vortex formation.

As vortex burst comes onto the wing, the associated positive pressure causes a nonlinearity in C_l. Burst occurs on the left wing first. Evidently, the deflected elevon (even for $\delta_L = -5$ deg) acts as Hummel's downstream obstacle,[7] causing earlier vortex burst. The pressure increase caused by burst is also realized on the fuselage, causing nonlinearities in C_Y and C_n. Eventually, as burst engulfs both wings, the lateral-directional stability coefficients tend toward zero.

Although flow photographs are shown only for $M = 0.9$, the flow phenomena are similar for transonic and low supersonic speeds. Flow separation grows linearly on the wing for $\delta_L > -25$ deg, giving linear control increments in C_l, C_m, C_Y, and C_n (Fig. 7). This holds true as long as the flow separation is vented only at the wing tip. However, once the separation is no longer contained under the orbital maneuvering system (OMS) pod, venting at the wing-fuselage juncture is also possible. This double venting essentially freezes the growth of the separated flow region and causes ΔC_l and ΔC_m to level off at $\delta_L < -25$ deg. However, the venting at the fuselage causes sidewash on the tail, which combines with the increased separation extent on the fuselage sides to increase ΔC_n and ΔC_Y also at $\delta_L < -25$ deg.

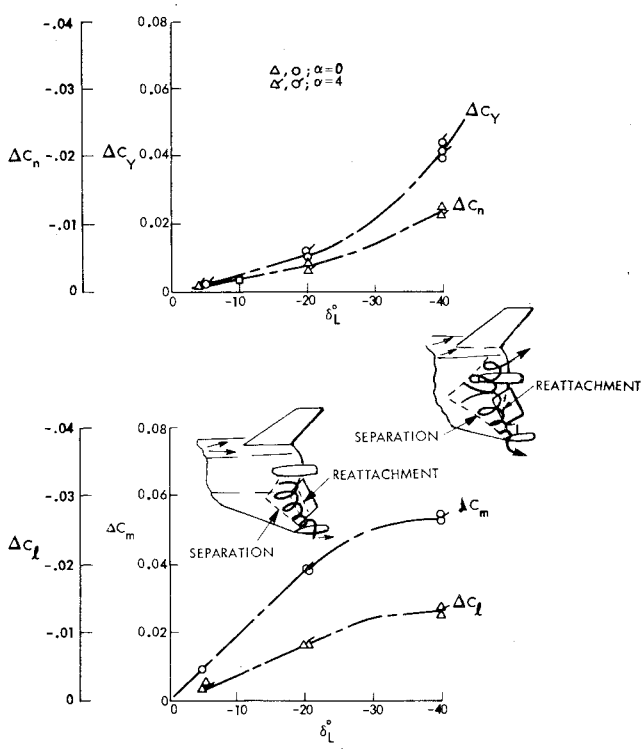

Fig. 7 NASA designed (040A) orbiter elevon effectiveness at $M = 1.46$.

The Current Orbiter

The current orbiter exhibits three distinct wing flow patterns (Fig. 8)[8,9] that dominate both the static and dynamic stability. At low angles of attack, separation occurs at the wing body juncture, resulting from the OMS pod induced adverse pressure gradient (Fig. 8a). A shock emanates from the separation. This shock merges with the OMS pod shock near the wing tip, causing a local flow separation. At some critical angle of attack, the wing-fuselage separation jumps to the strake apex, generating a strake-fuselage vortex that affects the wing loads (Fig. 8b). Simultaneously, the forward wing shock becomes strong enough to cause its own flow separation. Finally, at high angles of attack, the strake-fuselage and strake-leading-edge vortices roll up together as the outboard wing panel stalls (Fig. 8c). It is significant that boundaries of the various flow phenomena correlate with nonlinearities in both static[10,11] and dynamic[12,13] stability characteristics (Fig. 9).

At transonic speeds, the orbiter dynamic stability data[12,13] (Fig. 10) exhibit the opposition between static and dynamic derivatives, which is indicative of a flowfield time lag[14] (stable $C_{mq} + C_{m_{\dot{\alpha}}}$ excursions correlate with unstable C_{m_α} excursions and vice versa). The sharp peaks in the derivatives suggest the possibility of highly nonlinear or discontinuous aerodynamic characteristics. Evidence from the oil-flow photographs (Fig. 8) indicates that the corner separation at the wing-fuselage juncture dominates the orbiter wing loads.

The strong forward wing shock, which forms when the corner separation jumps to the strake apex, produces a relatively high pressure region of flow separation. The high pressure causes a statically destabilizing download on the orbiter wing which accounts for the unstable spikes in C_{m_α} at $\alpha = 2$ deg (Fig. 10). As the strake vortex increases in strength, it produces increasingly negative suction pressures over the wing, increasing the static stability for 4 deg $\leq \alpha \leq$ 12 deg.

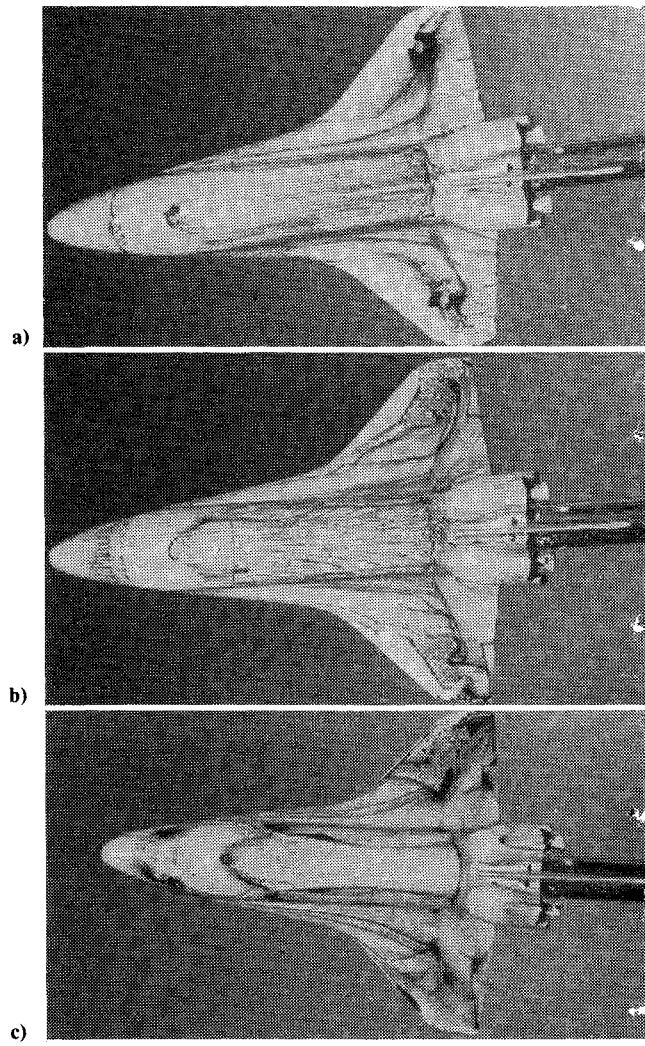

Fig. 8 Orbiter leeside flow patterns. a) $\alpha = 5$ deg. b) $\alpha = 10$ deg. c) $\alpha = 20$ deg.

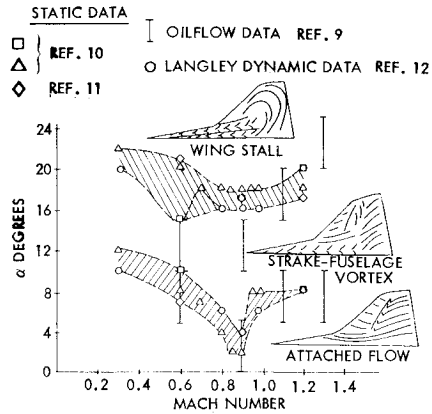

Fig. 9 Correlation of data nonlinearities with oil-flow results.

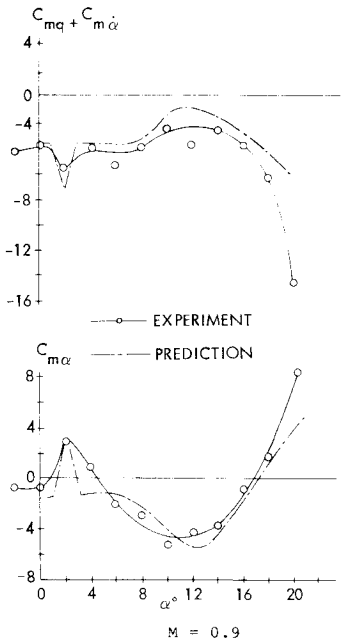

Fig. 10 Orbiter dynamics at transonic speeds.

Eventually, as the wing stalls at $\alpha > 12$ deg, the static stability diminishes, becoming unstable for $\alpha = 18$ deg.

Using the measured static stability characteristics and accounting for the flowfield time lag effects, the dynamic stability characteristics have been determined,[15,16] showing agreement with the experimental dynamic data (Fig. 10). Thus the nonlinear dynamic stability characteristics could be successfully predicted from the experimental static stability data, using an analytic technique that accounts for the flowfield time lag associated with the strake-fuselage vortex. The development of this mathematical model was a direct result of the insight into the flowfield gained from the flow visualization results.

Conclusions

Flow visualization techniques have given important insight into the causes of a variety of nonlinear aerodynamic effects that have dominated the entire spectrum of Shuttle orbiters. These techniques are equally useful in the design of high performance aircraft as they are frequently geometrically similar to the Space Shuttle, with low aspect ratio wing-strake planforms; they also fly at high angles of attack in order to achieve high load factor maneuvers. Thus simple flow visualization techniques should continue to be a powerful tool for diagnosing complicated flow phenomena.

References

[1] Seegmiller, H.L., "Shadowgraphs and Surface Flow Visualization Photographs of the MSC Orbiter at Mach No. 7.4," NASA SSPD-3, Jan. 13, 1970.

[2] Reding, J.P. and Ericsson, L.E., "Unsteady Aerodynamics Analysis of Manned Space Vehicles; Past, Present and Future," *Proceedings of the First Western Space Congress,* Santa Maria, Calif., Oct. 27-29, 1970, pp. 882-893.

[3] Seegmiller, H.L., "Surface Flow Visualization Investigation of a High Cross Range Shuttle Configuration at a Mach Number of 7.4 and Several Reynolds Numbers," NASA TM X-62036, June 2, 1970.

[4] Cross, E.J., "Analytical Investigation of the Expansion Flow Field Over a Delta Wing at Hypersonic Speeds," Aerospace Research Laboratory, Wright-Patterson Air Force Base, Ohio, ARL 68-0027, Feb. 1968.

[5] Reding, J.P. and Ericsson, L.E., "Review of Delta Wing Space Shuttle Vehicle Dynamics," Space Shuttle Aero-Thermodynamics Technology Conference, Volume III, Aerodynamics; see also NASA TM X-2508, Feb. 1972, pp. 861-921.

[6] Reding, J.P. and Ericsson, L.E., "Unsteady Aerodynamic Analysis of Space Shuttle Vehicles, Part IV: Effect of Control Deflections on Orbiter Unsteady Aerodynamics," Lockheed Missiles and Space Company, Inc., LMSC/D352320, Aug. 1973.

[7] Hummel, D., "Untersuchungen uber das Aufplatzen der Wirbel an Schlanken Delta-Flugeln," *Zeitschrift fuer Flugwissenschaften* Vol. 13, 1956, pp. 159-168.

[8] Reding, J.P. and Ericsson, L.E., "Unsteady Aerodynamic Flow Field Analysis of the Space Shuttle Configuration. Part II: Launch Vehicle Aeroelastic Analysis," Lockheed Missiles and Space Company, Inc., LMSC/D057194, April 1976.

[9] Nichols, M.E., "Results of Investigation of the 0.004-Scale Model 74-0 of the Configuration 4 (Modified) Space Shuttle Orbiter in the NASA/MSFC 14 by 14 Inch, Trisonic Wind Tunnel (0A131)," NASA CR 141521, March 1975.

[10] Allen, E.C. and Lindhall, R.H., "Investigation in the MSFC TWT to Verify the Static Stability and Control Effectiveness of the 0.004-Scale Model (74.0) of the Shuttle 5 Orbiter (0A-108)," NASA CR 141537, June 1975.

[11] Sparks, V.H. and Moser, M.M. Jr., "Wind Tunnel Tests of an 0.015-Scale Configuration 140 A1B Space Shuttle Orbiter Model (67-0) in the NASA LRC 8-foot TPT to Obtain Transonic Aerodynamic Force Data (0A-106)," NASA CR 134426, June 1975.

[12] Boyden, R.P. and Freeman, D.C., "Subsonic and Transonic Dynamic Stability Derivatives of a Modified 089B Shuttle Orbiter," NASA TM X-72631, Dec. 1974.

[13] Freeman, D.C. Jr., Boyden, R.P., and Davenport, E.E., "Supersonic Dynamic Stability Derivatives of a Modified 089B Shuttle Orbiter," NASA TM X-72630, Oct. 1974.

[14] Ericsson, L.E. and Reding, J.P., "Analysis of Flow Separation Effects on the Dynamics of a Large Space Booster," *Journal of Spacecraft and Rockets,* Vol. 4, July-Aug. 1965, pp. 481-490.

[15] Reding, J.P. and Ericsson, L.E., "Effects of Flow Separation on Shuttle Longitudinal Dynamics and Aeroelastic Stability," *Journal of Spacecraft and Rockets,* Vol. 14, Dec. 1977, pp. 711-718.

[16] Ericsson, L.E. and Reding, J.P., "Effect of Flow Separation Vortices on Aircraft Unsteady Aerodynamics," Paper 24, AGARD CP-235, May 1978, pp. 24-1—24-12.